

Metal-Promoted Aromatic Ring Amination and Deamination Reactions at a Diazo Ligand Coordinated to Rhodium and Ruthenium

Chayan Das,[†] Amit K. Ghosh,[†] Chen-Hsiung Hung,[‡] Gene-Hsiang Lee,[§] Shie-Ming Peng,[§] and Sreebrata Goswami^{*†}

Department of Inorganic Chemistry, Indian Association for the Cultivation of Science, Kolkata 700 032, India, Department of Chemistry, National Changhua University of Education, Changhua, Taiwan 500, Republic of China, and Department of Chemistry, National Taiwan University, Taipei, Taiwan, Republic of China

Received June 24, 2002

Reactions of $MCl_3 \cdot 3H_2O$ ($M = Rh$ and Ru) with the ligand 2-[(2-*N*-arylamino)phenylazo]pyridine [HL^1 ; $NH_4C_5N=NC_6H_4N(H)C_6H_4(H)$ (HL^{1a}), $NH_4C_5N=NC_6H_4N(H)C_6H_4(CH_3)$ (HL^{1b}), and $NH_4C_5N=NC_6H_4N(H)C_5H_4N$ (HL^{1c})] in the presence of dilute NEt_3 afforded multiple products. In the case of rhodium, two green compounds, viz. $[Rh(L^1)_2]^+$ ($[2]^+$) and $[RhCl(pap)(L^1)]^+$ ($[3]^+$), where L^1 and pap stand for the conjugate base of $[HL^1]$ and 2-(phenylazo)pyridine, respectively, were separated on a preparative thin layer chromatographic plate. The reaction of $RuCl_3 \cdot 3H_2O$, on the other hand, produced two brown compounds, viz. $[RuCl(HL^1)(L^1)]$ (**4**) and $[RuCl(pap)(L^1)]$ (**5**), respectively, as the major products. The X-ray structures of the representative complexes are reported. Except for complex **2**, and **4**, the products are formed due to the cleavage of an otherwise unreactive C(phenyl)–N(amino) bond. In complex **4**, one of the tridentate ligands (HL^1) does not use its maximum denticity and coordinates as a neutral bidentate donor. Plausible reasons for the differences in their modes of coordination of the ligands as in **2** and **4** have been discussed. The ligand pap in the cationic mixed ligand complex $[3]^+$ reacts instantaneously with $ArNH_2$ to produce an ink-blue compound, $[RhCl(HL^2)(L^1)]^+$ ($[6]^+$) in a high yield. The ligand HL^2 is formed due to regioselective fusion of $ArNH_2$ residue at the para carbon of the phenyl ring (with respect to the azo fragment) of pap in $[3]^+$. The above complexes are generally intensely colored and show strong absorptions in the visible region, which are assigned to intraligand charge transfer transitions. These complexes undergo multiple and successive one-electron-transfer processes at the cathodic potentials. Electrogenerated cationic complexes of ruthenium(III), $[4]^+$ and $[5]^+$, showed rhombic EPR spectra at 77 K.

Introduction

The chemical reactions that are associated¹ with bond-making and bond-breaking processes in organic molecules have been of immense interest. In this respect, the reactions of coordinated ligands are important.² In fact, these provide facile synthetic routes for the synthesis of many novel

molecules, which are otherwise difficult, or in some cases even impossible, to synthesize following conventional synthetic procedures. In the recent years we have noted a number of metal-promoted C–N bond forming processes^{3–12} includ-

* Author to whom correspondence should be addressed. Fax: (+91) 33-473 2805. E-mail: icsg@mahendra.iacs.res.in.

[†] Indian Association for the Cultivation of Science.

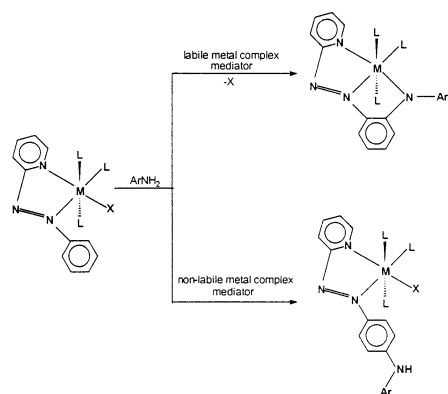
[‡] National Changhua University of Education.

[§] National Taiwan University.

- (1) See, for example: (a) Hartwig, J. F. *Acc. Chem. Res.* **1998**, *31*, 852. (b) Lockwood, M. A.; Fanwick, P. E.; Einentein, O.; Rothwell, I. P. *J. Am. Chem. Soc.* **1996**, *118*, 2762. (c) Lahiri, G. K.; Goswami, S.; Falvello, L. R.; Chakravorty, A. *Inorg. Chem.* **1987**, *26*, 3365. (d) Li, Z.; Quan, R. W.; Jacobsen, E. N. *J. Am. Chem. Soc.* **1995**, *117*, 5889. (e) Kuwabe, S.; Torraca, K. E.; Buchwald, S. L. *J. Am. Chem. Soc.* **2001**, *123*, 12202.

- (2) Selected leading references: (a) Hegedus, L. S. *Coord. Chem. Rev.* **1997**, *161*, 129. (b) Hegedus, L. S. *Coord. Chem. Rev.* **1998**, *168*, 49. (c) Hegedus, L. S. *Coord. Chem. Rev.* **1998**, *175*, 159. (d) Naota, T.; Takaya, H.; Murahashi, S.-I. *Chem. Rev.* **1998**, *98*, 2599. (e) Black, D. St. C. *Comprehensive Coordination Chemistry*; Wilkinson, G., Ed.; Pergamon: Oxford, 1987; Vol. 1, p 415. (f) Black, D. St. C. *Comprehensive Coordination Chemistry*; Wilkinson, G., Ed.; Pergamon: Oxford, 1987; Vol. 6, p 155. (g) Kondo, T.; Okada, T.; Mitsudo, T. *J. Am. Chem. Soc.* **2002**, *124*, 186. (3) Mitra, K. N.; Goswami, S. *Inorg. Chem.* **1997**, *36*, 1322. (4) Mitra, K. N.; Majumdar, P.; Peng, S.-M.; Castiñeiras, A.; Goswami, S. *Chem. Commun.* **1997**, 1267. (5) Mitra, K. N.; Peng, S.-M.; Goswami, S. *Chem. Commun.* **1998**, 1685. (6) Mitra, K. N.; Choudhury, S.; Castiñeiras, A.; Goswami, S. *J. Chem. Soc., Dalton Trans.* **1998**, 2901.

Scheme 1



ing the fusion of aromatic amines at a coordinated diazo ligand, 2-(phenylazo)pyridine (pap). We note here that amination of an aromatic ring that occurs with C–N bond formation is difficult but is a synthetically useful reaction.

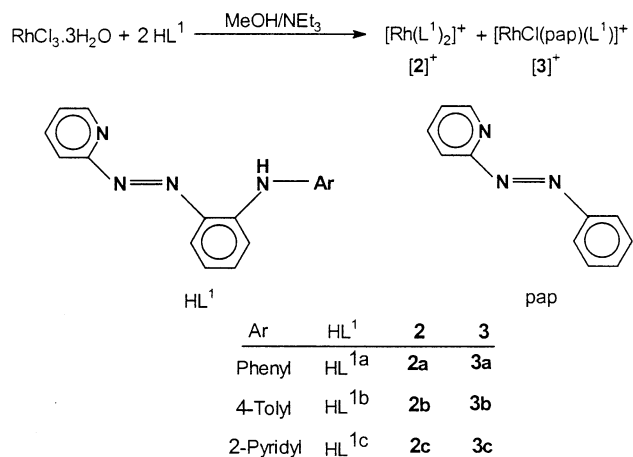
In the course of our investigations on the amination of pap ligands in M–pap complexes, we were concerned with the site selectivity of the fusion of ArNH₂ at the pendant phenyl ring of the coordinated diazo ligand (Scheme 1). We recently have noted⁹ that one of the two pap ligands in the rhodium complex [RhCl₂(pap)₂]⁺ ([1]⁺) undergoes amination at the ortho carbon to result in a tridentate ligand, while the second pap ligand in the above rhodium complex is aminated at the para carbon and thus produces a bidentate ligand. These results have prompted us to look further into the above fusion reactions. To understand the reasons for the site selection of the above amination reaction, we have designed and carried out the chemical reactions starting from some chosen rhodium substrates. In this context, we found it worthwhile to compare the results with the ruthenium analogues. Bivalent ruthenium is isoelectronic with trivalent rhodium; however, the properties of these two are vastly different, which has been useful for understanding the above fusion reactions of coordinated pap ligands.

The primary aim of this paper is to look into the aromatic amine fusion reactions of metal-coordinated pap ligand. These have been followed by the isolation of the intermediates as well as the final products. In all cases, identifications of the products are made, beyond doubt, by use of single-crystal X-ray structure analysis.

Results and Discussion

Reaction of Preformed HL¹ and RhCl₃·3H₂O. We first consider the products obtained from the reaction of the preformed tridentate ligand HL¹ with hydrated RhCl₃. The

Scheme 2



ligand HL¹ was obtained¹³ by the regioselective ortho-aromatic amination of coordinated pap ligand to a cobalt(II) center. The reaction (Scheme 2) in boiling methanol produced a green solution in about 4 h. Two green products **2** and **3** were isolated from the crude mixture on a preparative silica gel thin-layer chromatographic (TLC) plate. The presence of dilute NEt₃ is necessary for the above reaction; otherwise the yields of the products **2** and **3** become negligible. These cationic compounds were obtained as their chloride salts, and the complexes **2c** and **3a** were found¹⁴ to be suitable for X-ray structural work.

Compound **2** was eluted as the first green band with chloroform–acetonitrile (2:1) mixture as the eluent and was obtained in ca. 35% yield. The ORTEP plot and atom numbering scheme for the cationic part of **2c** are shown in Figure 1. Selective bond distances are collected in Table 1. The structural analysis of the cationic [Rh(L^{1c})₂]⁺ reveals the presence of two [L^{1c}][−] ligands, each of which acts as an *N,N,N*-tridentate donor with deprotonation of the amine nitrogens, viz. N(2) and N(7). The pyridyl nitrogens N(1) and N(6) remain uncoordinated. The geometry of the cationic complex is meridional, and the Rh atom sits on an imposed C₂ axis bisecting the angles N(5)–Rh–N(10) and N(2)–Rh–N(7). The two azo nitrogen atoms of the anionic tridentate ligands approach the metal center more closely [Rh–N(3)/N(8) average 1.962(4) Å] than the other four Rh–N bonds. There is an indication of significant backbone conjugation in the coordinated [L^{1c}][−] ligand. Thus the N=N azo distances (average 1.291(5) Å) in this complex are appreciably elongated. The main features of the structure of **2c** are similar to those for the complexes^{11,13} of [L^{1a}][−] involving 3d-metal ions, [M(L¹)₂]⁺ [M = Co(III), Fe(III)].

The second green band was eluted by the same solvent mixture and was obtained in ca. 30% yield. The color of this **3** is similar to that of compound **2**. The compound **3a** formed suitable X-ray quality crystals for structure determination. Figure 2 shows the ORTEP plot and atom

- (7) Ghosh, A. K.; Mitra, K. N.; Mostafa, G.; Goswami, S. *Eur. J. Inorg. Chem.* **2000**, 1961.
 (8) Majumdar, P.; Falvello, L. R.; Tomas, M.; Goswami, S. *Chem. Eur. J.* **2001**, *7*, 5222.
 (9) Saha, A.; Ghosh, A. K.; Majumdar, P.; Mitra, K. N.; Mondal, S.; Rajak, K. K.; Falvello, L. R.; Goswami, S. *Organometallics* **1999**, *18*, 3372.
 (10) Ghosh, A. K.; Majumdar, P.; Falvello, L. R.; Mostafa, G.; Goswami, S. *Organometallics* **1999**, *18*, 5086.
 (11) Saha, A.; Majumdar, P.; Peng, S.-M.; Goswami, S. *Eur. J. Inorg. Chem.* **2000**, 2631.
 (12) (a) Wolfe, J. P.; Wagaw, S.; Marcoux, J.-F.; Buchwald, S. L. *Acc. Chem. Res.* **1998**, *31*, 805. (b) Hartwig, J. F. *Angew. Chem., Int. Ed.* **1998**, *37*, 2046.

- (13) Saha, A.; Majumdar, P.; Goswami, S. *J. Chem. Soc., Dalton Trans.* **2000**, 1703.

- (14) After repeated trials we could grow X-ray quality crystals of **2c**. The compounds **2a** and **2b** are crystalline but did not produce suitable X-ray quality crystals.

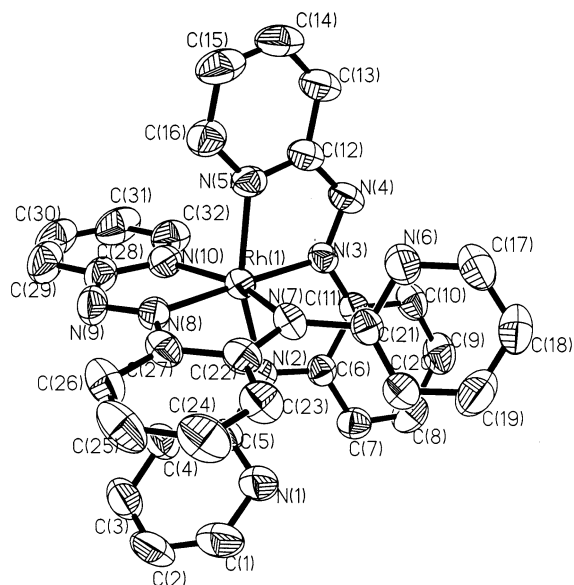


Figure 1. ORTEP plot and atom numbering scheme for the cationic part of the complex **2c**. Hydrogen atoms are not shown for clarity.

Table 1. Selected Bond Distances (Å)

2c					
Rh(1)–N(5)	2.043(4)	C(12)–N(4)	1.397(6)	C(28)–N(9)	1.393(7)
Rh(1)–N(3)	1.965(4)	N(4)–N(3)	1.288(5)	N(9)–N(8)	1.293(5)
Rh(1)–N(2)	2.036(4)	N(3)–C(11)	1.366(6)	N(8)–C(27)	1.348(6)
Rh(1)–N(10)	2.053(4)	C(11)–C(6)	1.436(6)	C(27)–C(22)	1.447(6)
Rh(1)–N(8)	1.958(4)	C(6)–N(2)	1.346(5)	C(22)–N(7)	1.335(6)
Rh(1)–N(7)	2.037(4)	N(2)–C(5)	1.421(5)	N(7)–C(21)	1.419(6)
N(5)–C(12)	1.377(6)	N(10)–C(28)	1.374(6)		
3a					
Rh(1)–N(1)	2.047(3)	N(1)–C(5)	1.366(4)	N(4)–C(12)	1.423(4)
Rh(1)–N(3)	1.941(3)	C(5)–N(2)	1.394(4)	N(5)–C(22)	1.356(4)
Rh(1)–N(4)	2.045(3)	N(2)–N(3)	1.298(4)	C(22)–N(6)	1.379(4)
Rh(1)–N(5)	2.052(3)	N(3)–C(6)	1.366(4)	N(6)–N(7)	1.266(4)
Rh(1)–N(7)	2.011(3)	C(6)–C(11)	1.416(5)	N(7)–C(23)	1.433(4)
Rh(1)–Cl(1)	2.3337(9)	C(11)–N(4)	1.342(4)		
4a					
Ru–N(1)	2.091(2)	C(22)–N(6)	1.372(3)	C(5)–N(2)	1.382(3)
Ru–N(3)	1.940(2)	N(6)–N(7)	1.316(3)	N(2)–N(3)	1.308(3)
Ru–N(4)	2.044(2)	N(7)–C(23)	1.438(3)	N(3)–C(6)	1.378(3)
Ru–N(5)	2.065(2)	C(27)–C(28)	1.404(3)	C(6)–C(11)	1.423(3)
Ru–N(7)	1.950(2)	C(28)–N(8)	1.379(3)	C(11)–N(4)	1.355(3)
Ru–Cl	2.3923(9)	N(8)–C(29)	1.415(4)	N(4)–C(12)	1.428(3)
N(5)–C(22)	1.354(3)	N(1)–C(5)	1.365(3)		
5a					
Ru–N(1)	2.086(6)	N(1)–C(5)	1.357(8)	N(4)–C(12)	1.421(8)
Ru–N(3)	1.933(5)	C(5)–N(2)	1.364(8)	N(5)–C(22)	1.368(8)
Ru–N(4)	2.038(6)	N(2)–N(3)	1.312(7)	C(22)–N(6)	1.360(8)
Ru–N(5)	2.068(5)	N(3)–C(6)	1.372(8)	N(6)–N(7)	1.314(7)
Ru–N(7)	1.933(5)	C(6)–C(11)	1.406(9)	N(7)–C(23)	1.432(7)
Ru–Cl	2.391(2)	C(11)–N(4)	1.353(8)		
6d					
Rh(1)–N(4)	2.048(5)	C(14)–N(3)	1.378(9)	N(5)–C(23)	1.360(9)
Rh(1)–N(2)	1.937(6)	N(3)–N(2)	1.313(7)	C(23)–N(6)	1.408(9)
Rh(1)–N(1)	2.042(5)	N(2)–C(13)	1.351(8)	N(6)–N(7)	1.278(8)
Rh(1)–N(5)	2.055(6)	C(13)–C(8)	1.421(9)	N(7)–C(24)	1.427(8)
Rh(1)–N(7)	2.056(6)	C(8)–N(1)	1.359(9)	C(27)–N(8)	1.364(9)
Rh(1)–Cl(1)	2.3427(18)	N(1)–C(5)	1.415(8)	N(8)–C(30)	1.436(9)
N(4)–C(14)	1.391(8)				

numbering scheme for the cationic part of the salt **3a**. Analysis of the crystal structure indeed authenticated the formation of a mixed ligand compound, $[\text{RhCl}(\text{pap})(\text{L}^1)]^+$, from the reaction as shown in Scheme 2. One of the two HL^1 ligands here has undergone a deamination reaction with the cleavage of a C–N bond to form the bidentate neutral

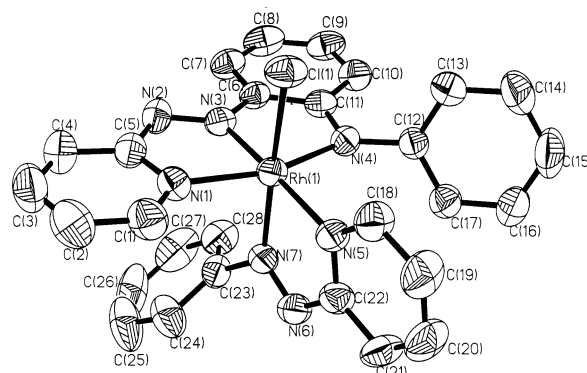
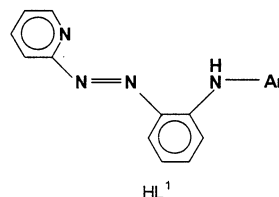
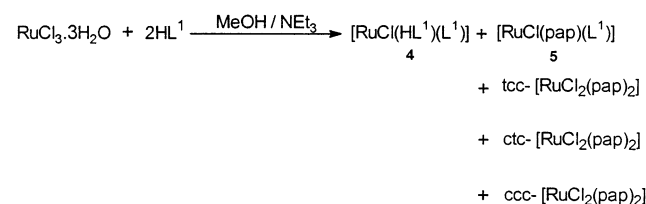


Figure 2. ORTEP plot and atom numbering scheme for the cationic part of the complex **3a**. Hydrogen atoms are not shown for clarity.

Scheme 3



Ar	HL^1	4	5
Phenyl	HL^{1a}	4a	5a
4-Tolyl	HL^{1b}	4b	5b

pap ligand. Notably, the relative geometry of the pairs of azo nitrogens in **2** is trans while that in **3** is cis. Finally, we wish to note that the N–N distance in the anionic extended ligand $[\text{L}^{1a}]^-$ is appreciably longer $[\text{N}(2)–\text{N}(3), 1.298(4) \text{ \AA}]$ than that $[\text{N}(6)–\text{N}(7), 1.266(4) \text{ \AA}]$ in the neutral pap ligand. This is attributed to the strong electron delocalization in $[\text{L}^{1a}]^-$ along the ligand backbone. Selected bond distances are collected in Table 1. Moreover, we wish to note here that the M–N distances with the middle nitrogen of coordinated terpyridyl and other related N, N, N donors are usually shorter than the other two M–N lengths.^{15,16} However, there is no indication of π -interactions between rhodium(III) and the neutral pap ligand.

During chromatographic purification, a small dark green brown band remained uneluted near the spot, which could not be purified so far.

Reaction of Preformed HL^1 and $\text{RuCl}_3 \cdot 3\text{H}_2\text{O}$. The reaction of hydrated RuCl_3 with HL^1 in boiling methanol in the presence of dilute NEt_3 produced a brown solution in about 5 h. Two new brown compounds **4** and **5** and three isomers of the known $[\text{RuCl}_2(\text{pap})_2]$ were isolated from the crude product using a preparative TLC separation technique (Scheme 3). Compound **4** was eluted as the first brown band

(15) (a) Britovsek, G. J. P.; Gibson, V. C.; Kimberley, B. S.; Mastroianni, S.; Redshaw, C.; Solan, G. A.; White, A. J. P.; Williams, D. J. *J. Chem. Soc., Dalton Trans.* **2001**, 1639. (b) Cadierno, V.; Gamasa, M. P.; Gimeno, J.; Iglesias, L.; García-Granda, S. *Inorg. Chem.* **1999**, *38*, 2874. (c) Pramanik, N. C.; Pramanik, K.; Ghosh, P.; Bhattacharya, S. *Polyhedron* **1998**, *17*, 1525.

(16) Jahng, Y.; Thummel, R. P.; Bott, S. G. *Inorg. Chem.* **1997**, *36*, 3133.

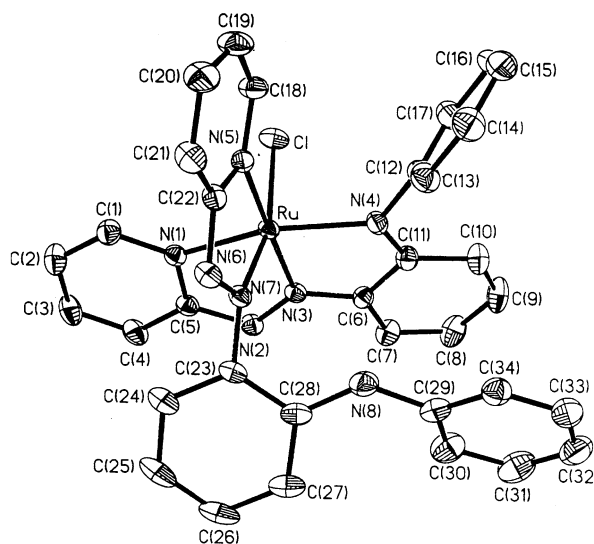


Figure 3. ORTEP plot and atom numbering scheme for the molecular complex **4a**. Hydrogen atoms are not shown for clarity.

with benzene–chloroform mixture (3:2) as the eluent and was obtained in ca. 10% yield. The unsubstituted compound **4a** formed suitable X-ray quality crystals for structure determination. An ORTEP plot along with atom numbering scheme for **4a** is shown in Figure 3. It shows that the coordination modes of attachment of the two ligands to the central ruthenium(II) ion are different. While one of these acts as a monoanionic tridentate ligand and chelates through N(1), N(3), and N(4), the other one acts as a neutral tridentate ligand and chelates to the metal ion via pyridine nitrogen N(5) and the azo nitrogen N(7). The neutral ligand thus bears a pendant arylamino group. The sixth coordination site of the central metal ion is occupied by a chloride ion providing a distorted octahedral $[\text{RuN}_5\text{Cl}]$ coordination environment. The relative positions of the pairs of pyridyl nitrogen and azo nitrogen in this complex are both *cis*. In this geometry, the amine N(8) is far from the metal center for coordination. Notably, the relative orientations of the coordinated atoms in **4** are different from that in the rhodium complex **2**. The extensive π -bonding from metal to ligand in **4a** is clear from the bond distance data of the compound (Table 1). Among the five Ru–N bonds the two Ru–N(azo) bonds, viz. Ru–N(3) and Ru–N(7), are shorter compared to other three Ru–N bonds. The N–N distances [1.308(3) Å (N(2)–N(3)) and 1.316(3) Å (N(6)–N(7))] are longer¹⁷ than those in $[\text{papH}]\text{ClO}_4$. These facts are indications of (a) delocalization of electronic charge of the anionic ligand, $[\text{L}^1]^-$, along the ligand backbone and (b) strong π -interactions between the metal d-orbitals and the neutral ligand $[\text{HL}^1]$ via its azo functionality.

The color of compound **5** is also brown; **5** was separated from the first brown band **4** on a preparative silica gel TLC plate using same solvent mixture as the eluent. These two bands overlap each other and were separated only upon allowing sufficient time for the separation. This was obtained in ca. 20% yield. Elemental analysis of compound **5** and its

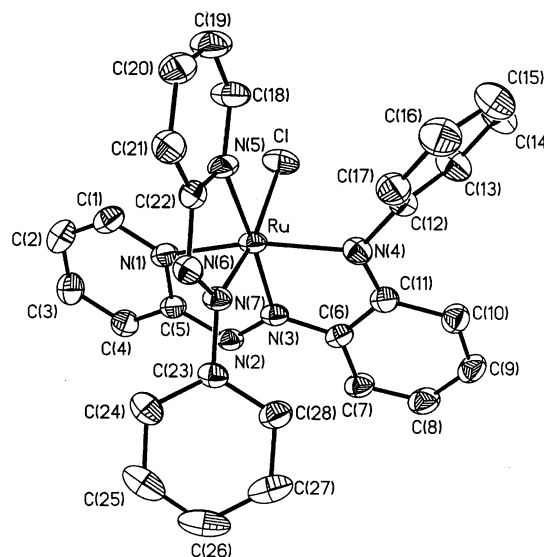


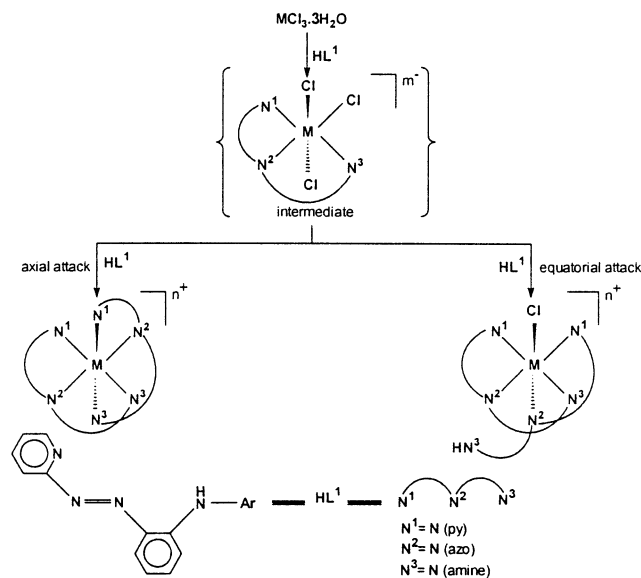
Figure 4. ORTEP plot and atom numbering scheme for the molecular complex **5a**. Hydrogen atoms are not shown for clarity.

¹H NMR spectra indicated the loss of an aromatic amine group from the ligand. The structural analysis of **5a** revealed that its composition corresponds to a mixed ligand complex, $[\text{RuCl}(\text{pap})(\text{L}^{1a})]$. In this compound, the ligand pap is formed due to deamination of HL^{1a} . The physicochemical properties of this compound are similar to those of compound **4**. Also, bond distances data (Table 1) show similar strong metal–ligand π -interactions. The ORTEP plot and atom numbering scheme for **5a** are shown in Figure 4. It may be noted here that the geometry of the molecular complex **5** is identical to that of the cationic rhodium complex **3**. It may be relevant to compare the bond lengths of the two related complexes **3a** and **5a**. In these two complexes, the metal centers are surrounded by a distorted octahedral coordination environment with one chloride ligand, the bidentate neutral chelating ligand, pap, and the tridentate monoanionic bischelating ligand, $[\text{L}^{1a}]^-$. The bond lengths of both **3a** and **5a**, along the ligand backbone of the coordinated $[\text{L}^{1a}]^-$, indicate extensive delocalization. As a result, (a) the N=N lengths are elongated, (b) azo nitrogen to phenyl carbon lengths are shorter than those in pap, and (c) the bond lengths of amine nitrogens to the phenyl group of pap are shorter than a C–N single bond. However, such delocalization was not observed in the neutral pap ligand. Interestingly, the Ru–N (azo, pap) distance, in **5a**, is notably shorter than the Ru–N (py, pap) distance. Moreover, the N–N distance (pap) is elongated appreciably. This is attributed to strong $d\pi$ – $p\pi$ interactions between Ru(II) and π^* (azo) of pap. Such metal–ligand interaction was, however, absent in **3a**. In this compound Rh–N (azo, pap) and Rh–N (py, pap) lengths are comparable and consequently the N–N distance (pap) retains its double bond character.¹⁷

Besides the aforementioned two brown compounds, the three known isomers of $[\text{RuCl}_2(\text{pap})_2]$, viz. *tcc*- $[\text{RuCl}_2(\text{pap})_2]$, *ctc*- $[\text{RuCl}_2(\text{pap})_2]$, and *ccc*- $[\text{RuCl}_2(\text{pap})_2]$, were also formed. These were separated on a silica gel TLC plate using chloroform as the eluent. The yields of these compounds varied between 5% and 10%. Their spectroscopic and

(17) Saha, A.; Das, C.; Peng, S.-M.; Goswami, S. *Indian J. Chem., Sect. A* **2001**, *40*, 198.

Scheme 4



voltammetric data exactly corresponded to those of the authentic samples of the known isomeric $[RuCl_2(\text{pap})_2]$. We also noted a few more minor bands on the TLC plate; none of these produced any detectable pure compound. In the above synthetic reaction involving $RuCl_3 \cdot 3H_2O$ and HL^1 , the starting trivalent ruthenium salt underwent one-electron reduction in methanol. The mechanism and the byproducts of the above reduction $[Ru(III) \rightarrow Ru(II)]$ are not established. However, we believe that complex formation followed by reduction¹⁸ would be a plausible path for the formation of bivalent ruthenium complexes.

Except for the first brown compound **4**, the rest of the ruthenium compounds, described above, are obtained due to the cleavage of at least one C(phenyl)–N(amine) bond in HL^1 . This organic transformation was not observed in the absence of metal ion.

Comparison between Schemes 2 and 3. The two types of products of undissociated $HL^1/[L^1]^-$ were obtained from the above two reactions. While in the case of ruthenium one of the two coordinated ligands does not use its maximum denticity, the ligands are symmetrically chelated in the rhodium complex, $[Rh(L^1)_2]^+$. It is known¹⁶ that the substitution reactions in $[MCl_3 \cdot 3H_2O]$ ($M = Ru, Rh$) proceed stepwise. Thus the product $\{[MCl_3(L^1)]^{m-}\}$ may be viewed as the intermediate complex for the above reactions (Scheme 4). This intermediate complex has one equatorial and two axial leaving groups (Cl), which are substituted by another $HL^1/[L^1]^-$ to form the final product. An axial attack by the terminal pyridyl(N) at the intermediate complex would produce a bischelate $[M(L^1)_2]^{n+}$, whereas an equatorial attack would lead to the mixed ligand complex $[MCl(L^1)(L^1)]^{n+}$. Thus it may be concluded that while axial attack is favored in the case of rhodium, the equatorial attack is preferred for ruthenium. It may be recalled here that in all its known complexes^{11,13} with 3d-metal ions, the ligand, under consid-

eration, binds as an anionic tridentate donor to yield metal complexes of the general formula $[M(L^1)_2]^{n+}$. In order to look for the differences, we also note that *trans*-N(azo), N(azo) pair orientation^{19,20} has never been observed in the ruthenium(II) complexes of pap ligands. The *trans*-M[N(azo), N(azo)] grouping is however, an essential prerequisite for the formation of $[M(L^1)_2]^{n+}$ complex. Unlike the 3d-metal ions, the ruthenium(II) ion is known to enter into π -interactions effectively with the low-lying π^* (ligand) orbitals. Thus, very strong $d\pi$ – $\text{azo}(\pi^*)$ back-bonding is a persistent feature in Ru(II)–pap chelates. In the *trans*-N(azo), N(azo) pair geometry, the $\pi^*(\text{azo})$ orbitals compete for the same metal $d\pi$ orbital, which weakens back-bonding. The rhodium(III) ion, on the other hand, is not a good π -donor and behaves like 3d-metal ions. Notably, osmium(II) also behaves²¹ like ruthenium(II) in its reaction with HL^1 .

Compounds **3** and **5** and the three isomers of $[RuCl_2(\text{pap})_2]$ are formed due to cleavage²² of at least one C(phenyl)–N(amine) bond. The mechanism for this bond cleavage reaction has not been elucidated. We note here that the ligand HL^1 reacts spontaneously with 3d-metal ions, where no such C–N bond cleavage was observed.^{11,13}

Amination Reaction. The mixed ligand complexes $[MCl(\text{pap})(L^1)]^{n+}$ ($M = Rh^{III}$, **3** ($n = 1$); $M = Ru^{II}$, **5** ($n = 0$)) contain coordinated pap ligand, and it was anticipated⁹ that these might be suitable substrates for amination reactions. In line with our strategy, both the complexes **3a** and **5a** were reacted with $ArNH_2$ neat and in the presence of air. While compound **3a** reacted instantaneously to produce an ink blue product, the corresponding ruthenium complex **5a** is unreactive to $ArNH_2$. Compounds **3a** and **5a** are similar except that the former is cationic while the latter is a molecular complex. Although $[5a]^+$ can be generated in solution by the exhaustive electrolysis of **5a**, we could not isolate $[5a]^+$ in its pure state. Thus it is concluded that amination reaction is facilitated²³ in a cationic complex, whose electrophilicity is higher than that for a molecular complex. Interestingly, the ink blue product, obtained from the reaction of **3a** and $ArNH_2$, is similar to the product obtained directly from the reaction of $[RhCl_2(\text{pap})_2]^+$ and $ArNH_2$. It was proposed^{9,24} that dissociation of a chloride ion from $[RhCl_2(\text{pap})_2]^+$ creates a vacant site and is hence responsible for ortho-amination of one of the two pap ligands in the starting rhodium dichloro complex. The second chloride ion could not be dissociated under our experimental conditions, and hence the amination

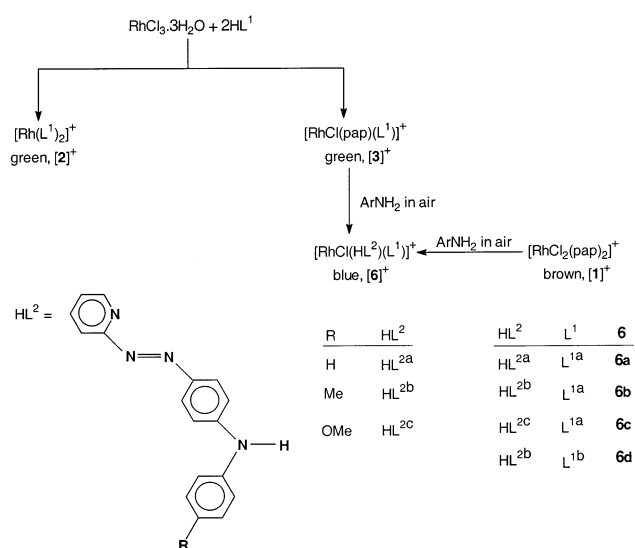
(18) (a) Goswami, S.; Chakravarty, A. R.; Chakravorty, A. *Inorg. Chem.* **1981**, *20*, 2246. (b) Choudhury, S.; Kakoti, M.; Deb, A. K.; Goswami, S. *Polyhedron* **1992**, *11*, 3183.

(19) (a) Seal, A.; Ray, S. *Acta Crystallogr., Sect. C* **1984**, *40*, 929. (b) Krause, K.; Krause, R. A.; Larsen, S.; Rasmussen, B. *Acta Chem. Scand. Ser. A* **1985**, *39*, 375. (c) Majumdar, P.; Peng, S.-M.; Goswami, S. *J. Chem. Soc., Dalton Trans.* **1998**, 1569. (d) Velders, A. H.; Kooijman, H.; Spak, A. L.; Haasnoot, J. G.; Vos, D. de; Reedijk, J. *Inorg. Chem.* **2000**, *39*, 2966.
 (20) Ghosh, B. K.; Mukhopadhyay, A.; Goswami, S.; Ray, S.; Chakravorty, A. *Inorg. Chem.* **1984**, *23*, 4633.
 (21) Das, C.; Peng, S.-M.; Lee, G.-H.; Goswami, S. *New J. Chem.* **2002**, *26*, 222.
 (22) (a) Bhattacharyya, S.; Weakley, T. J. R.; Chaudhury, M. *Inorg. Chem.* **1999**, *38*, 5433. (b) Gray, S. D.; Weller, K. J.; Bruck, M. A.; Briggs, P. M.; Wigley, D. E. *J. Am. Chem. Soc.* **1995**, *117*, 10678.
 (23) Kamar, K. K.; Saha, A.; Castiñeiras, A.; Hung, C.-H.; Goswami, S. *Inorg. Chem.* **2002**, *41*, 4531. Das, C.; Saha, A.; Hung, C.-H.; Lee, G.-H.; Peng, S.-M.; Goswami, S. *Inorg. Chem.* **2003**, *42*, 0000.
 (24) Deb, A. K.; Goswami, S. *J. Chem. Soc., Dalton Trans.* **1989**, 1635.

Table 2. Spectral Data

compd	IR, ^a cm ⁻¹			absorption ^b λ _{max} , nm (ε, M ⁻¹ cm ⁻¹)
	ν(N–H)	ν(C=N)	ν(N=N)	
2a		1600	1310	890 (7370), 795 (11 350), 725 (11 240), 655, ^c 440, ^c 350 (19 890), 255 ^d (36 160)
2b		1595	1325	900 (6270), 800 (9710), 735 (9520), 660, ^c 435, ^c 355 (16 120), 265 ^d (30 930)
2c		1595	1310	885 (5670), 790 (8960), 715 (8240), 645, ^c 430, ^c 350 (15 800), 275 (23 560)
3a		1610	1320, 1435	895 (3870), 800 (6840), 730 (6330), 660, ^c 360 (18 320), 265 ^d (25 250)
3b		1610	1320, 1430	900 (3280), 800 (5770), 735 (5360), 665, ^c 365 (15 250), 265 ^d (21 640)
3c		1600	1310, 1435	890 (3090), 790 (5610), 720 (4790), 650, ^c 350 (13 140), 275 (16 390)
4a	3390	1595	1233, 1295	950 ^d (3310), 830 (4380), 555 ^d (6190), 470 (9410), 375, ^c 290 (29 180)
4b	3405	1595	1230, 1275	960 ^d (3150), 830 (4340), 555 ^d (6350), 470 (9420), 390, ^c 290 (29 330)
5a		1595	1230, 1275	970 ^d (3450), 850 (4450), 555 (7050), 475 (10 280), 300 (22 030)
5b		1595	1225, 1270	990 ^d (3620), 850 (5060), 550 (7400), 475 (10 980), 300 (23 080)
6a	3410	1585	1310, 1435	910 (3020), 805 (5500), 605 (28 910), 395, ^c 355 ^d (11 620), 270 (25 230)
6b	3400	1585	1310, 1440	915 (2820), 810 (5150), 605 (25 500), 400, ^c 350 ^d (10 500), 280 (21 600)
6c	3405	1585	1315, 1440	910 (2910), 805 (5500), 605 (24 860), 400, ^c 360 (11 830), 275 (26 560)
6d	3410	1590	1315, 1440	910 (2720), 805 (4940), 610 (27 660), 395, ^c 340 ^d (16 260), 270 (26 920)

^a In KBr disk. ^b In acetonitrile. ^c Ill-defined shoulder. ^d Shoulder.

Scheme 5

of the second pap in the said complex occurs at the para position as the second choice. Our present results have indeed confirmed our proposition. Compound **3**, in fact, is the proposed intermediate for the transformation $[\text{RhCl}_2(\text{pap})_2]^+ \rightarrow [\text{RhCl}(\text{HL}^2)(\text{L}^1)]^+ ([\mathbf{1}]^+ \rightarrow [\mathbf{6}]^+)$. The results have been summarized in Scheme 5.

The reaction of **3a** with three different aromatic amines, ArNH_2 ($\text{ArNH}_2 = \text{aniline}, p\text{-toluidine}, \text{and } p\text{-anisidine}$) produced a deep blue mixture, which on chromatographic purification yielded the ink blue crystalline compound **6** in >75% yield. The compound $[\text{RhCl}(\text{HL}^{2b})(\text{L}^{1b})](\text{PF}_6)$ (**6d**) formed crystals suitable for the determination of its X-ray structure. In this complex, the extended ligand HL^{2b} is neutral and is formed due to fusion of *p*-toluidine fragment to the coordinated pap ligand in **3b** at the para position (relative to the azo fragment) of the phenyl group of pap. This acts as a bidentate ligand and chelates to rhodium through the pyridine nitrogen N(5) and the azo nitrogen N(7). The amine nitrogen atom N(8) of this bears a hydrogen atom and remains uncoordinated. The bidentate HL^{2b} and anionic tridentate $[\text{L}^{1b}]^-$ along with one chloride ion complete a distorted octahedral environment about rhodium.⁹ A comparison of bond distance data in this molecule (Table 1)

indicates different levels of conjugation in the two coordinated ligands. For example, the N–N distance for the neutral HL^{2b} , N(6)–N(7), is 1.278(8) Å while the corresponding distance in the anionic tridentate ligand $[\text{L}^{1b}]^-$, N(2)–N(3), is 1.313(7) Å. Taken together, the lengthening of the azo N=N distance in $[\text{L}^{1b}]^-$ and the foreshortening of the N–C distances alongside the azo moiety, with respect to the corresponding distances in HL^{2b} itself, indicate greater delocalization of π -electron density in $[\text{L}^{1b}]^-$. The central Rh–N bond of the anionic ligand, Rh(1)–N(2) = 1.937(6) Å, is significantly shorter than the other four Rh–N lengths, which are all near their average value of 2.050(5) Å.

Furthermore, the mixed rhodium(III) complex $[\text{RhCl}(\text{pap})(\text{L}^1)]^+$ (**3**) is substitutionally inert, from which chloride ion dissociation was not possible. The amination reaction in this substitutionally inert complex occurs exclusively at the para carbon of the pendant phenyl ring of coordinated pap.

Spectral Properties. Selected spectral data are collected in Table 2. The features of the IR spectra of the complexes are closely similar to those of the reported examples.^{9,11,13} The N=N stretching frequencies are lowered. The ¹H NMR spectra of the bis chelated compounds, **2**, are resolved. Notably, each kind of proton of the coordinated ligand $[\text{L}^1]^-$ gave rise to one signal confirming the presence of a 2-fold symmetry axis. The rest of the compounds **3–6** are all mixed ligand complexes that are coordinated by different ligands. As a result, these gave rise to complex spectral patterns due to the presence of large numbers of unique protons. While the methyl resonances of HL^{1b} and HL^{2b} appeared in the range 2.15–2.35 δ, in HL^{2c} (OCH_3) it appeared near 3.90 δ.

Figure 6 shows the solution spectra of the representative examples. Multiple low-energy transitions are the characteristics of all the spectra (Table 2). The solution color of the two rhodium complexes, viz. **2** and **3**, are green while that for **6** is ink blue. The spectral patterns of the compounds **2** and **3** are similar except that the intensities of the low-energy transitions (900–650 nm) for compound **2** are roughly double the intensities of similar transitions for compound **3**. It is to be noted here that while compound **2** is coordinated by the two anionic tridentate ligands $[\text{L}^1]^-$, compound **3**, on the other hand, has only one such ligand.

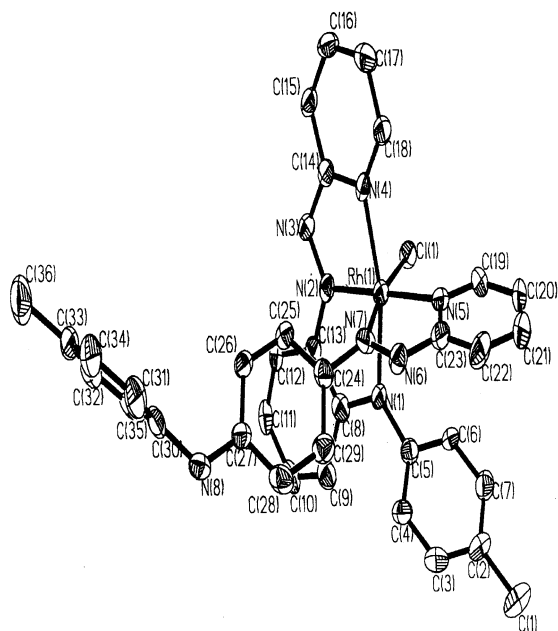


Figure 5. ORTEP plot and atom numbering scheme for the cationic part of the complex **6d**. Hydrogen atoms are not shown for clarity.

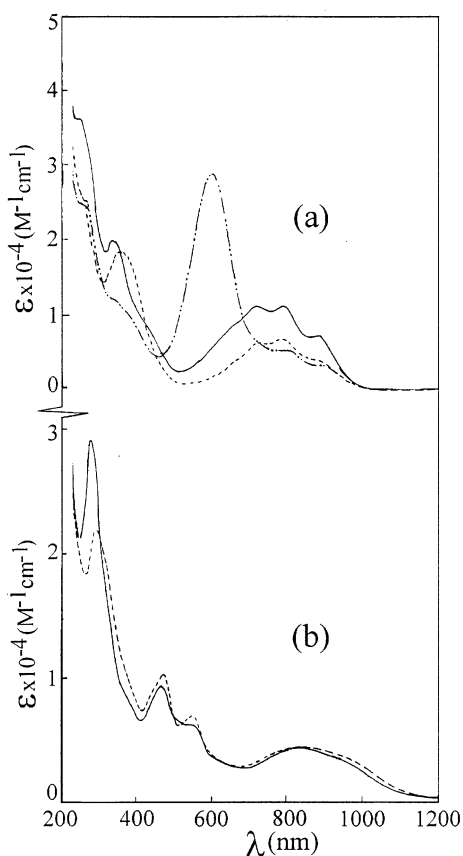


Figure 6. Electronic spectra of (a) **2a** (—), **3a** (---), and **6a** (- · - ·); and (b) **4a** (—) and **5a** (---).

These results tempt us to propose that these low-energy transitions in **2** and **3** involve orbitals that are predominantly ligand in character and originated primarily from the coordinated $[L^1]^-$ ligand part. We have performed extended Hückel MO calculations with the crystallographic parameters

of **2c**, **3a** and **6d**, using the CACAO program²⁵ by Mealli and Proserpio. Due to the obvious limitations, we note that the results are qualitative in nature. However, the calculations have indicated that the HOMO and HOMO - 1 orbitals in these complexes are predominantly ligand orbitals with only small contributions from the metal orbitals (Supporting Information Figure S1). The acceptor orbital LUMO is also a ligand orbital with ca. 20% contribution from the metal d-orbitals. Interestingly, on moving from **3** to **6** the spectral nature is completely changed (Figure 6a). Two low-energy transitions are observed in **6**. The lowest energy transitions in the range (900–800 nm) are similar, in both intensity and energy, to that observed in **3**. The transition near 730 nm (in **3**), however, is replaced by a highly intense transition ($\epsilon > 25\,000\text{ M}^{-1}\text{ cm}^{-1}$) near 605 nm, which is responsible for the intense ink blue color of compound **6**. In fact, the blue color is characteristic²³ of all the transition metal complexes that contain HL^2 as a ligand. In the ligand, HL^2 , a donor amine group is separated from an acceptor azo function by a conjugated spacer. The acceptor ability of the azo chromophore is expected to be augmented on coordination. Hence the transition near 605 nm in the complexes **6** is assigned to an intraligand transition localized at the coordinated HL^2 ligand. We wish to note here that such low-energy transitions in rhodium(III) complexes are virtually unknown.²⁶

The spectra of the ruthenium complexes consist of similar two low-energy transitions in the range (1000–820 nm), which are red shifted compared to those of the rhodium(III) complexes. Notably, two additional strong transitions near 550 and 475 nm were also observable (Figure 6b). The ruthenium(II) complexes containing acceptor ligands in general show²⁷ intense metal-to-ligand charge transfer (MLCT) in the visible region. The above transitions may be ascribed to MLCT transitions. Notably, in addition to the multiple-step ligand reductions, metal oxidation redox processes were observable only in the ruthenium complexes (vide infra).

Redox Properties. Both the free ligands HL^1 and HL^2 are known to undergo¹¹ two-step reductions in the range -1.20 to -2.00 V. These also show an irreversible anodic wave near 1.05 V due to their oxidation.

The cyclic voltammograms of the rhodium complexes are dominated by the multiple step reduction processes (Table 3, Figure 7). The anodic responses, on the other hand, are irreversible. All the redox processes in the rhodium complexes involve²⁴ primarily ligand orbitals.

The voltammograms of the ruthenium complexes **4** and **5** are almost identical. In fact, the two ruthenium complexes are similar with the exception that in **4** an ortho-substituted ligand HL^1 replaces the pap ligand. The *o*-arylamino substitution on pap appears to have a very minor effect on the redox and the spectral properties of the reference complexes. The cathodic responses in the ruthenium com-

(25) Mealli, C.; Proserpio, D. M. *J. Chem. Educ.* **1990**, *67*, 399.

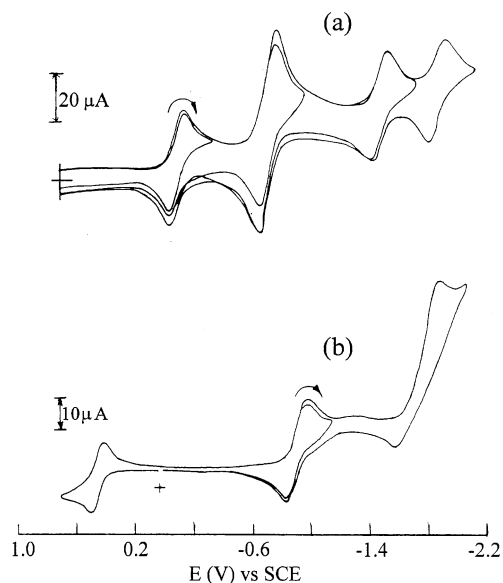
(26) Cotton, F. A.; Wilkinson, G.; Murillo, C. A.; Bochmann, M. *Advanced Inorganic Chemistry*, 6th ed.; Wiley: New York, 1999; p 1048.

(27) (a) Kober, E. M.; Meyer, T. J. *Inorg. Chem.* **1982**, *21*, 3967. (b) Goswami, S.; Mukherjee, R.; Chakravorty, A. *Inorg. Chem.* **1983**, *22*, 2825.

Table 3. Cyclic Voltammetric Data^a

compd	$E_{1/2},^b$ V (ΔE_p , mV)	$-E_{1/2},^b$ V (ΔE_p , mV)
2a	1.42 ^c	0.48 (70), 0.81 (100), 1.45 (120), 1.75 (120)
2b	1.33 ^c	0.50 (70), 0.81 (90), 1.43 (100), 1.73 (100)
2c	1.49 ^c	0.43 (60), 0.71 (80), 1.35 (100), 1.73 (100)
3a	1.32 ^c	0.07 (90), 0.69 (100), 1.43 (100), 1.83 (100)
3b	1.25 ^c	0.21 (90), 0.75 (90), 1.18 (100), 1.41 (110)
3c	1.39 ^c	0.10 (70), 0.62 (100), 1.32 (100), 1.71 (120)
4a	0.46 (90), 1.42 ^d	0.91, ^e 1.17, ^e 1.72 ^e
4b	0.45 (70), 1.40 ^d	0.90, ^e 1.14, ^e 1.70 ^e
5a	0.46 (80), 1.25 ^d	0.90 (150), 1.87 ^e
5b	0.45 (100), 1.19 (100)	0.89, ^d 1.85 ^e
6a	1.33 ^c	0.25 (80), 0.58 (120), 0.82 (70), 1.48 (110), 1.80 (130)
6b	1.30 ^c	0.25 (90), 0.54 (120), 0.82 (80), 1.42 (120), 1.76 (140)
6c	1.26 ^c	0.25 (90), 0.55 (110), 0.83 (90), 1.45 (100), 1.75 (120)
6d	1.27 ^c	0.25 (90), 0.52 (100), 0.80 (70), 1.50 (90), 1.78 (120)

^a Conditions: solvent, acetonitrile; supporting electrolyte, NETClO_4 , (0.1 M); working electrode, platinum for oxidation and glassy carbon for reduction processes; reference electrode SCE; solute concentration, ca. 10^{-3} (M); scan rate, 50 mV s^{-1} . ^b $E_{1/2}$, the redox processes are reversible. $E_{1/2}$ is calculated as the average of anodic (E_{pa}) and cathodic (E_{pc}) peak potentials. $\Delta E_p = E_{pa} - E_{pc}$ in mV. ^c E_{pa} , irreversible anodic response. ^d Quasireversible. ^e E_{pc} , irreversible cathodic response.

**Figure 7.** Segmented cyclic voltammograms of (a) **3a** and (b) **5a** in CH_3CN (0.1 M TEAP); scan rate 50 mV s^{-1} .

plexes are also due to^{27–29} the reductions of the coordinated ligands. Notably, these responses shift anodic appreciably in the corresponding complexes of rhodium(III) (Table 3). This shift is due to higher electrophilicity of the cationic rhodium(III) complexes¹⁰ over the neutral ruthenium complexes. The first reversible oxidative anodic responses in the ruthenium(II) complexes near 0.45 V are due to the $\text{Ru}^{\text{II}}/\text{Ru}^{\text{III}}$ redox process.

Low potentials of $\text{Ru}^{\text{II}}/\text{Ru}^{\text{III}}$ couples, in **4** and **5**, persuaded us to try to isolate the corresponding ruthenium(III) compounds in their pure states. Accordingly, attempts were made to oxidize them both chemically and electrochemically.

(28) Krejčík, M.; Zálíš, S.; Klíma, J.; Sýkora, D.; Matheis, W.; Klein, A.; Káim, W. *Inorg. Chem.* **1993**, *32*, 3362.

(29) Ghosh, B. K.; Chakravorty, A. *Coord. Chem. Rev.* **1989**, *95*, 239.

Unfortunately, the oxidized complexes were not stable enough and revert to the parent bivalent complexes. However, we were successful at generating two representatives of the cationic complexes, viz. $[\mathbf{4a}]^+$ and $[\mathbf{5a}]^+$, in solution by the controlled potential bulk electrolysis of **4a** and **5a**. Well-resolved rhombic spectra of the above ruthenium complexes $[\mathbf{4a}]^+$ and $[\mathbf{5a}]^+$ were obtained in frozen (77 K) dichloromethane–toluene solution. The details are given in the Experimental Section.

The EPR data are collected in Table 4, and the representative spectra are shown in Figure 8. The observed rhombicity of the EPR spectra in the present cases is understandable in terms of the gross molecular symmetry of these complexes, containing three nonequivalent axes.³⁰ The rhombic distortion can be thought of as a combination of axial distortion (Δ , which splits t_2 into a and e) and rhombic distortion (V , which splits e). Spin–orbit coupling causes further changes in the energy gaps. Thus, two electronic transitions of transition energies ΔE_1 and ΔE_2 ($\Delta E_1 < \Delta E_2$) are, in principle, probable within these three levels. All these energy parameters for the above low spin ruthenium(III) complexes have been computed³¹ using the observed g -values. The axial distortion is much stronger than the rhombic one (Table 4). The analyses of the EPR spectral data thus indicate that both $[\mathbf{4a}]^+$ and $[\mathbf{5a}]^+$ are significantly distorted from ideal octahedral arrangements, which indeed is in agreement with the observed structures of the parent bivalent complexes.

The ΔE_1 and ΔE_2 transitions have been observed in the expected near-IR region and visible region, respectively. In view of approximations of the theory, the agreement between the calculated and observed transition energies is satisfactory.

Conclusion

Some examples of fascinating metal-promoted transformations, viz. amination and deamination at the pendant phenyl ring of coordinated 2-(phenylazo)pyridine, have been followed by the careful design of chemical reactions. The multiple products, from each of the reactions, have been purified and completely characterized. Electronic as well as kinetic reasons for the formation of the mixed ligand ruthenium complex $[\text{RuCl}(\text{HL}^1)(\text{L}^1)]$ (**4**) as against the bis chelate, $[\text{Rh}(\text{L}^1)_2]\text{Cl}$ (**2**) have been noted. The deaminated products, particularly in the cases of rhodium, are found to be useful for the study of amination reactions. Regioselectivity of the amination reaction has been proven. The complexes thus formed show rich spectral as well as redox properties, which have been thoroughly investigated. Most notable is the appearance of intense intraligand charge-transfer transitions in the low-energy part of the visible region. The aminated organic ligands, in general, have both donor and acceptor chromophores, which are separated by the conjugated spacers. The complexes of these are under active scrutiny and might be useful in the development³² of nonlinear optically active materials.

(30) Reiger, P. H. *Coord. Chem. Rev.* **1994**, *135/136*, 203.

(31) Bhattacharya, S.; Chakravorty, A. *Proc. Indian Acad. Sci., Chem. Sci.* **1985**, *95*, 159 and references therein.

Table 4. Electronic Spectra and EPR Data of the Cationic Compounds [4a]⁺ and [5a]⁺

compd	electronic spectra ^a λ_{\max} , cm ⁻¹	EPR <i>g</i> values ^c and derived energy params, ^d cm ⁻¹						
		<i>g</i> ₁	<i>g</i> ₂	<i>g</i> ₃	Δ	<i>V</i>	ΔE_1	ΔE_2
[4a] ⁺	7930, 11 900, 15 430, ^b 19 530, 27 320, 35 460	2.1437	2.0792	1.9699	10 330	4800	7970	12 850
[5a] ⁺	8200, 11 620, 19 450, 27 620, 32 470 ^b	2.1367	2.0726	1.9729	10 950	5430	8280	13 780

^a Qualitative spectra in acetonitrile. ^b Shoulder. ^c In 1:1 dichloromethane–toluene solution at 77 K. ^d Taking the value of spin–orbit coupling constant (λ) for low-spin ruthenium(II) as equal to 1000 cm⁻¹.

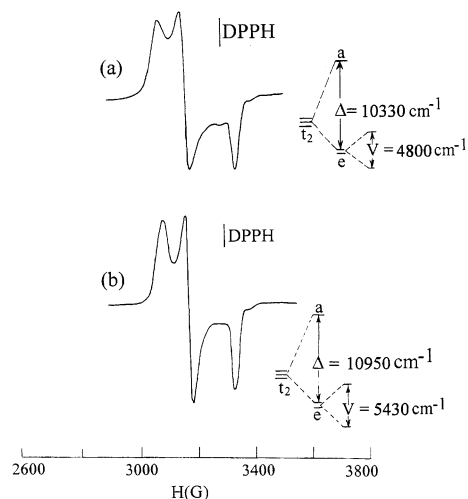


Figure 8. EPR spectra of (a) **4a** and (b) **5a** in 1:1 dichloromethane–toluene solution at 77 K, also showing computed splittings of *t*₂ orbitals. DPPH = diphenylpicrylhydrazyl.

Experimental Section

Materials. The starting metal salts RhCl₃·3H₂O and RuCl₃·3H₂O were digested thrice with concentrated HCl before use. The ligand HL¹ and [RhCl₂(pap)₂]ClO₄ were prepared following the reported^{13,24} procedure. Solvents and chemicals used for the syntheses were of analytical grade.

Physical Measurements. Microanalytical data (C, H, N) were collected from a Perkin–Elmer 240C elemental analyzer. A Perkin–Elmer 783 spectrophotometer was used for the measurement of IR spectral data. The ¹H NMR spectral data were recorded with a Bruker Avance 300 spectrophotometer using SiMe₄ as an internal standard. Electrochemical measurements were performed at 298 K under a dry nitrogen atmosphere on a PC-controlled PAR Model 273A electrochemistry system. A platinum disk, a platinum wire auxiliary electrode, and an aqueous saturated calomel reference electrode (SCE) were used in a three-electrode configuration. The *E*_{1/2} for the ferrocenium–ferrocene couple under our experimental condition was 0.39 V. Electronic spectral data were recorded on a JASCO V-570 spectrophotometer. EPR spectral measurements were done on a Varian Model 109C E-line X-band spectrometer fitted with a quartz Dewar for measurement at 77 K, and all spectral data were calibrated against the spectrum of DPPH.

Reactions of RhCl₃·3H₂O with HL¹. The reactions of RhCl₃·3H₂O with different substituted ligands (HL^{1a}–HL^{1c}) were performed similarly to synthesize the compounds [Rh(L¹)₂]Cl **2** and [RhCl(pap)(L¹)]Cl **3**, where [L¹]⁻ is the conjugate base of HL¹. A detail of a representative reaction with HL^{1a} is elaborated below.

Isolation of [Rh(L^{1a})₂]Cl (2a**) and [RhCl(pap)(L^{1a})]Cl (**3a**).** To a reddish brown mixture of RhCl₃·3H₂O (0.23 g, 0.88 mmol)

and HL^{1a} (0.48 g, 1.76 mmol) in 60 mL of methanol, 2 drops of NEt₃ was added. The mixture was refluxed on a steam bath. The color of the solution gradually turned green in 1/2 h. The reaction was continued for 4 h for completion. The resultant solution was cooled and filtered. On evaporation of the green filtrate a dark mass was obtained, which was then loaded on a preparative silica gel TLC plate for separation. The solvent mixture chloroform–acetonitrile (2:1) was used as the eluent. Two green bands **2a** and **3a** were separated. A dark greenish brown band was observed at the spot, which remained uneluted even with acetonitrile. The isolated green compounds were finally recrystallized from dichloromethane–hexane solvent mixture.

2a. Yield: 0.21 g, 35%. Anal. Calcd for C₃₄H₂₆N₈ClRh: C, 59.62; H, 3.83; N, 16.36. Found: C, 59.57; H, 3.61; N, 16.25. MS: *m/z* 649 [M – Cl]⁺.

3a. Yield: 0.16 g, 29%. Anal. Calcd for C₂₈H₂₂N₇Cl₂Rh: C, 53.35; H, 3.52; N, 15.55. Found: C, 53.53; H, 3.72; N, 15.61. MS: *m/z* 594 [M – Cl]⁺.

The yields and the analytical data of **2b**, **3b** and **2c**, **3c** are given below:

2b. Yield: 35%. Anal. Calcd for C₃₆H₃₀N₈ClRh: C, 60.64; H, 4.24; N, 15.71. Found: C, 60.51; H, 4.30; N, 15.55.

3b. Yield: 30%. Anal. Calcd for C₂₉H₂₄N₇Cl₂Rh: C, 54.05; H, 3.75; N, 15.22. Found: C, 54.15; H, 3.80; N, 15.32.

2c. Yield: 32%. Anal. Calcd for C₃₂H₂₄N₁₀ClRh: C, 55.95; H, 3.52; N, 20.39. Found: C, 55.84; H, 3.48; N, 20.31.

3c. Yield: 28%. Anal. Calcd for C₂₇H₂₁N₈Cl₂Rh: C, 51.37; H, 3.35; N, 17.75. Found: C, 51.32; H, 3.19; N, 17.64.

Reactions of RuCl₃·3H₂O with HL¹. The reactions of RuCl₃·3H₂O with HL^{1a} and HL^{1b} were performed by following a similar procedure. A detail of a representative is elaborated below.

Isolation of [RuCl(HL^{1a})(L^{1a})] (4a**) and [RuCl(pap)(L^{1a})] (**5a**).** To a reddish mixture of RuCl₃·3H₂O (0.23 g, 0.89 mmol) and HL^{1a} (0.49 g, 1.78 mmol) in 60 mL of methanol, 2 drops of NEt₃ was added. The mixture was refluxed on a steam bath for 5 h. The initial reddish color changed to dark brown during this period. The resultant solution was cooled and filtered. On evaporation of the filtrate a dark crude mass was obtained. It was washed thoroughly with diethyl ether. The crude mass was recrystallized several times from dichloromethane–hexane mixture. Then it was subjected to chromatography on a preparative silica gel TLC plate using a benzene–chloroform mixture (3:2) as the eluent. Two brown bands **4a** and **5a** were separated gradually after allowing sufficient time. The other byproducts, the three isomers of [RuCl₂(pap)₂], formed in this reaction were also isolated as distinct bands using chloroform as the eluent. Some minor brownish violet bands were also observed on the TLC plate, which could not be isolated in pure form.

4a. Yield: 0.07 g, 11%. Anal. Calcd for C₃₄H₂₇N₈ClRu: C, 59.69; H, 3.98; N, 16.38. Found: C, 59.48; H, 4.12; N, 16.23.

5a. Yield: 0.12 g, 23%. Anal. Calcd for C₂₈H₂₂N₇ClRu: C, 56.71; H, 3.74; N, 16.53. Found: C, 56.53; H, 3.90; N, 16.39.

The yields and analytical data of **4b** and **5b** are as follows:

4b. Yield: 12%. Anal. Calcd for C₃₆H₃₁N₈ClRu: C, 60.71; H, 4.39; N, 15.73. Found: C, 60.47; H, 4.19; N, 15.45.

(32) (a) Lacroix, P. G. *Eur. J. Inorg. Chem.* **2001**, 339. (b) Bozec, H. L.; Remouazd, T. *Eur. J. Inorg. Chem.* **2000**, 229. (c) Dhenaut, C.; Ledoux, I.; Samuel, I. D. W.; Zyss, J.; Bourgault, M.; Bozec, H. L. *Nature* **1995**, 374, 339. (d) Zyss, J.; Ledoux, I. *Chem. Rev.* **1994**, 94, 77.

Table 5. Crystal Data for Compound **2c**, **3a**, **4a**, **5a** and **6d**

	2c ·4H ₂ O	3a ·4H ₂ O	4a	5a	6d
empirical formula	C ₃₂ H ₃₂ ClN ₁₀ O ₄ Rh	C ₂₈ H ₃₀ Cl ₂ N ₇ O ₄ Rh	C ₃₄ H ₂₇ ClN ₈ Ru	C ₂₈ H ₂₂ ClN ₇ Ru	C ₃₆ H ₃₁ ClF ₆ N ₈ PRh
formula weight	759.04	702.40	684.16	593.05	859.02
temp [K]	293(2)	293(2)	295(2)	293(2)	150(2)
cryst syst	monoclinic	monoclinic	monoclinic	monoclinic	triclinic
space group	<i>P</i> 2(1)/ <i>n</i>	<i>P</i> 2(1)/ <i>c</i>	<i>P</i> 2(1)/ <i>n</i>	<i>P</i> 2(1)/ <i>n</i>	<i>P</i> 1
<i>a</i> [Å]	11.8962(7)	19.7142(11)	10.998(2)	13.481(7)	8.9645(8)
<i>b</i> [Å]	22.2032(14)	7.8744(4)	20.067(4)	14.377(9)	12.4699(12)
<i>c</i> [Å]	13.4009(8)	20.4434(11)	14.530(3)	13.543(7)	17.0283(17)
α [deg]	90	90	90	90	107.483(2)
β [deg]	105.7390(10)	101.5580(10)	110.26(2)	91.83(4)	104.519(2)
γ [deg]	90	90	90	90	92.834(2)
<i>Z</i>	4	4	4	4	2
<i>D</i> _{calcd} [mg/m ³]	1.480	1.501	1.511	1.502	1.638
cryst dimen [mm ³]	0.30 × 0.12 × 0.08	0.24 × 0.23 × 0.21	0.60 × 0.50 × 0.40	0.50 × 0.40 × 0.40	0.34 × 0.21 × 0.07
θ range for data collection [deg]	1.83–27.51	2.03–27.53	1.81–25	2.07–24.01	1.31–27.52
GOF	0.895	0.864	1.064	1.047	0.819
reflns collected	21 424	19 165	5295	4470	11 255
unique reflns	7746	7097	5295	4027	7761
final <i>R</i> indices [<i>I</i> > 2 σ (<i>I</i>)]	<i>R</i> 1 = 0.0485 w <i>R</i> 2 = 0.1343	<i>R</i> 1 = 0.0378 w <i>R</i> 2 = 0.0895	<i>R</i> 1 = 0.0252 w <i>R</i> 2 = 0.0645	<i>R</i> 1 = 0.0512 w <i>R</i> 2 = 0.1151	<i>R</i> 1 = 0.0506 w <i>R</i> 2 = 0.1071

5b. Yield: 22%. Anal. Calcd for C₂₉H₂₄N₇ClRu: C, 57.38; H, 3.98; N, 16.15. Found: C, 57.17; H, 4.11; N, 16.01.

Amination Reactions. Two different routes of amination reactions on coordinated pap ligand have been explored. In the first route we have described the amination reaction of coordinated pap in [RhCl(pap)(L¹)]Cl (**3**). The second method involves the reaction of [RhCl₂(pap)₂]ClO₄ (**1**) with different ArNH₂ compounds. The products, obtained from the two routes, are identical but the yields are different.

Method I. [3]⁺ → [6]⁺, a Representative Example: **Synthesis of [RhCl(HL^{2a})(L^{1a})]⁺, [6a]⁺.** A sample of [RhCl(pap)(L^{1a})]Cl (**3a**) (0.20 g, 0.32 mmol) was mixed with 0.5 mL of aniline, and the mixture was heated on a steam bath. The green mixture turned blue within 15 min. The reaction was continued for 3 h for the completion of the reaction. The mixture was then cooled and thoroughly washed with diethyl ether. A blue compound was purified on a preparative TLC plate (silica gel) using chloroform–acetonitrile mixture (3:1) as the eluent. Finally the compound, as its chloride salt, was recrystallized from dichloromethane–hexane solvent mixture. Yield: 0.18 g, 78%. Anal. Calcd for C₃₄H₂₇N₈Cl₂Rh: C, 56.60; H, 3.77; N, 15.53. Found: C, 56.47; H, 3.63; N, 15.42. MS: *m/z* 685 [M – Cl]⁺.

The yields and analytical data of **6b**, **6c**, and **6d** are given below.

6b. Yield: 78%. Anal. Calcd for C₃₅H₂₉N₈Cl₂Rh: C, 57.16; H, 3.97; N, 15.23. Found: C, 57.41; H, 4.12; N, 15.39. MS: *m/z* 699 [M – Cl]⁺.

6c. Yield: 75%. Anal. Calcd for C₃₅H₂₉N₈Cl₂ORh: C, 55.94; H, 3.89; N, 14.91. Found: C, 55.85; H, 3.80; N, 14.98.

6d. Yield: 80%. Anal. Calcd for C₃₆H₃₁N₈Cl₂Rh: C, 57.69; H, 4.17; N, 14.95. Found: C, 57.52; H, 4.01; N, 14.85.

Method II. [1]⁺ → [6]⁺, a Representative Example: **Synthesis of [RhCl(HL^{2a})(L^{1a})]⁺, [6a]⁺.** A mixture of [RhCl₂(pap)₂]ClO₄ (0.20 g, 0.31 mmol) and aniline (0.5 mL) was heated on a steam bath for 2 h. The cooled blue mixture was thoroughly washed with diethyl ether. The crude mass was purified on a preparative TLC plate (silica gel) using chloroform–acetonitrile solvent mixture (3:1) as the eluent. Recrystallization of the product from a dichloromethane–hexane solvent mixture yielded dark blue cationic compound **6a** as its perchlorate salt. Yield: 0.13 g, 55%. Anal. Calcd for C₃₄H₂₇N₈Cl₂O₄Rh: C, 51.99; H, 3.46; N, 14.26. Found: C, 51.73; H, 3.33; N, 14.02. MS: *m/z* 685 [M – ClO₄]⁺.

The cationic compound [6a]⁺ obtained following method II is identical to that obtained from method I. We, however, note that

the two ligands in the product **6** (method II) carries identical substitution, R, depending on the starting ArNH₂. The starting rhodium complex **3** is, in fact, the intermediate for the reaction **1** → **6** (vide supra). Hence the two ligands in the products, obtained from **3**, may not necessarily bear identical substitutions.

Electrochemical Generation of [4a]⁺ and [5a]⁺. The complexes [4a]⁺ and [5a]⁺ were generated in solution by constant potential coulometric oxidation of solutions of **4a** and **5a**, respectively. A detail of a representative example ([4a]⁺) is noted below.

A solution of 9.0 mg of **4a** in 30 mL of dichloromethane solvent containing 35 mg of tetrabutylammoniumperchlorate was oxidized coulometrically. The oxidation was performed at 0.65 V; *n* = 1.22/1.27 = 0.96, *n* = *Q*/*Q'*, where *Q* is the coulomb count found after exhaustive electrolysis and *Q'* is the calculated coulomb count for one-electron transfer. A part of the electrogenerated solution (5 mL) of [4a]⁺ was mixed with an equal volume of toluene, and the mixture was quickly frozen at 77 K and then used for an EPR measurement. The oxidized complex [4a]⁺ was not stable at room temperature. It underwent reduction to produce **4a** almost quantitatively. To date, we were not successful in isolating the trivalent ruthenium compound [4a]⁺ in its pure state.

The trivalent complex [5a]⁺ was generated in solution similarly as described above.

Crystallography. Crystallographic data for the compounds **2c**, **3a**, **4a**, **5a**, and **6d** are collected in Table 5. The suitable X-ray crystals of **2c** and **3a** were obtained by slow diffusion of a dichloromethane solution of chloride salt of **2c** and **3a** into hexane. The X-ray crystals of **6d** were obtained by slow diffusion of a dichloromethane solution of hexafluorophosphate salt of **6d** into hexane. Intensity data of all these three compounds (**2c**, **3a**, and **6d**) were collected on a Bruker SMART diffractometer, equipped with graphite monochromated Mo K α radiation, λ = 0.710 73 Å. These were corrected for Lorentz polarization effects. All three structures were solved by employing SHELXS-97³³ package of programs and refined by full matrix least squares based on *F*² (SHELXL-97).³⁴ The X-ray quality crystals of **4a** were obtained by the slow diffusion of a dichloromethane solution of **4a** into hexane. Intensity data were collected on a NONIUS CAD4 diffractometer, equipped with graphite monochromated Mo K α , λ

(33) Sheldrick, G. M. *Acta Crystallogr., Sect. A* **1990**, *46*, 467.

(34) Sheldrick, G. M. *SHELXL97, Program for the Refinement of Crystal Structures*; University of Göttingen: Göttingen, Germany, 1997.

Aromatic Ring Amination and Deamination Reactions

= 0.710 73 Å. The data were corrected for Lorentz polarization effects. The X-ray quality crystals of **5a** were grown by slow diffusion of a toluene solution of **5a** into hexane. Intensity data were collected on a Sieman R3m/V diffractometer with graphite monochromated Mo K α radiation, $\lambda = 0.710\ 73\ \text{\AA}$. All the data were corrected for Lorentz polarization effects. The structures of compounds **4a** and **5a** were solved by using the SHELXS-86 package³⁵ of programs and refined by full matrix least squares based on F^2 (SHELXL-93).³⁶ All the hydrogen atoms were added in calculated positions.

(35) Sheldrick, G. M. *SHELXS86, Program for the Solution of Crystal Structures*; University of Göttingen: Göttingen, Germany, 1990.

(36) Sheldrick, G. M. *SHELXL93, Program for the Refinement of Crystal Structures*; University of Göttingen: Göttingen, Germany, 1993.

Acknowledgment. Financial support received from the Department of Science and Technology and The Council of Scientific and Industrial Research (New Delhi) is gratefully acknowledged. We are thankful to Prof. Animesh Chakravorty and Dr. Samaresh Bhattacharya for help. Thanks are due to RSIC, Lucknow, for providing mass spectra.

Supporting Information Available: X-ray crystallographic details in CIF format of the five compounds **2c**, **3a**, **4a**, **5a**, and **6d**; molecular orbital diagram of **3a**: (a) LUMO, (b) HOMO, and (c) HOMO – 1. These materials are available free of charge via the Internet at <http://pubs.acs.org>.

IC020421C